THE JOURNAL OF PHYSICAL CHEMISTRY B

Article

pubs.acs.org/JPCB

Photoinduced Electron-Transfer Reactions of Carbonic Anhydrase Inhibitor Containing Tris(2,2′-bipyridine)ruthenium(II) Analogue

Hiroshi Takashima,* Misa Fukuda, Fumie Nakagaki, Tomoko Ogata, and Keiichi Tsukahara*

Department of Chemistry, Faculty of Science, Nara Women's University, Nara 630-8506, Japan

Supporting Information

ABSTRACT: A ruthenium(II) complex-based carbonic anhydrase (CA) inhibitor, $[Ru(bpy)_2(bpybs)]^{2+}$ {bpy = 2,2′-bipyridine and bpybs = 4′-methyl-2,2′-bipyridinyl-4-carboxylic acid (2-{2-[(4-sulphamoylbenzoyl-amino)ethoxy]ethoxy}ethyl)amide}, tethering a benzenesulfonamide group and a $[Ru(bpy)_3]^{2+}$ moiety has been prepared. The CA activity was effectively suppressed by a synthetic $[Ru(bpy)_2(bpybs)]^{2+}$ inhibitor, and the dissociation constant at pH 7.2 and at 25 °C was determined to be K_I = 1.9 ± 0.2 μM. Next, in the presence of CA and a sacrificial electron acceptor, such as pentaamminechlorocobalt(III) complex, the photoexcited triplet state of $^3([Ru(bpy)_2(bpybs)]^{2+})^*$ was quenched through an intermolecular photoinduced ET mechanism to form the oxidized $[Ru(bpy)_2(bpybs)]^{3+}$, followed by the intramolecular electron abstraction from an amino-acid residue near the active site of CA. The resulting oxidized CA was catalytically inactive. Kinetic experiments also revealed that the second-order rate constant for the initial step and the first-order rate constant for the second step under our experimental conditions were $k_q = 4.8 \times 10^7$ M^{-1} s^{-1} and $k_{IET} = 6.6 \times 10^4$ s^{-1}, respectively. Thus, the intramolecular ET between CA and $[Ru(bpy)_2(bpybs)]^{3+}$ is a crucial event to regulate CA activity by the visible light irradiation of a synthetic $[Ru(bpy)_3]^{2+}$-type inhibitor.

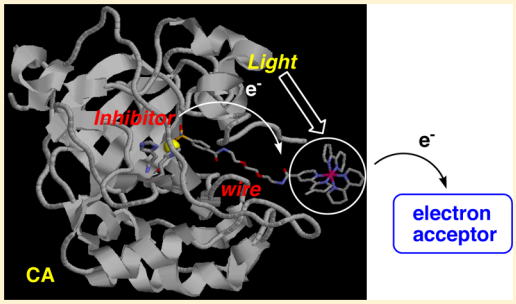

INTRODUCTION

Photoinduced electron-transfer (ET) reactions within a metalloprotein matrix to transport the electron initiated by the light have received considerable attention in the fields of both chemistry and biology.[1−7] Various mechanistic and design approaches based on photochemistry of metal complexes have been undertaken, and much effort on the intramolecular photoinduced ET reactions using hemoprotein has been carried out.[8,9] As a photosenzitizer, metal-substituted heme or ruthenium complex with polypyridyl ligands is utilized, because its photoexcited triplet state can act as a strong reductant having a long lifetime of microseconds.[10−14] To date, the semisynthetic reconstitution of zinc-substituted heme into apomyoglobin (Mb) has been a topic of interest.[15,16] Direct chemical modification of a heme propionate with a redox-active compound connected by a methylene "wire" spacer produces artificial intramolecular photoinduced ET systems of Mb.[8,16b,17,18] The reconstituted zinc-Mb (ZnMb), containing a covalently linked methylviologen (MV^{2+}) or acridinium ion,[19−21] confers the donor−acceptor dyad for the intramolecular ET reaction from the photoexcited singlet ^{1}(ZnMb)* or triplet ^{3}(ZnMb)*. In addition, we recently designed zinc(II)-protoporphyrin IX appending an ethylenediaminetetraacetic acid.[22] Its preferential transition metal complex showed metal-ion-dependent electron or energy transfer. These models realize fast photoinduced reaction within a protein scaffold and generate a long-lived charge separated state to elucidate the complicated mechanisms of photoinduced ET.

Instead of the above semisynthetic cofactor reconstitution strategies, one of the promising ways is to construct artificial ET systems of proteins by introducing a metal complex via specific protein−ligand interactions.[23,24] Gray et al. recently reported a molecular "wire" comprising a ruthenium(II) or rhenium(I) complex and an aromatic group that makes contact with the metalloenzyme active site.[25] The ruthenium−diimine complexes designed to bind to cytochrome P450cam were prepared by optimizing the interactions of the ruthenium group, the linker, and the active site recognition element with the protein. The intramolecular photoreduction of cytochrome P450cam by the Ru wires occurred via an ET pathway through an alkyl chain with 5 orders of magnitude faster than reduction by the natural redox partner, putidaredoxin.[25a,26] A similar effect on electron tunneling to the enzyme active site was observed for the aromatic wire molecule with copper amine oxidase.[27,28] It is also reported that these wire molecules showed enzyme inhibition activities by blocking the substrate channel to the active site.[25b,c,28]

Carbonic anhydrase (CA) is one of the popular zinc metalloenzymes that catalyze the reversible hydration of CO_2. The active site of CA contains a Zn^{2+} ion coordinated by three histidine residues at the bottom of a 15 Å cleft.[29,30] Since the synthetic inhibitor that binds to its deep cleft is stable at physiological conditions, CA was chosen as a model enzyme for

Received: October 26, 2012
Revised: February 8, 2013
Published: February 13, 2013

understanding protein−ligand interactions.[31,32] Many strong binding CA inhibitors containing a sulfonamide moiety that is coordinated to Zn^{2+} have developed, and their enzyme−inhibitor complexes have been crystallographically characterized.[32] In addition, some designed benzenesulfonamide-type inhibitors tethering a functional molecule have been used for biological applications. The synthetic benzenesulfonamide fluorophores can be used for selective recognition of Zn^{2+} ion in design of a CA-based fluorescent biosensor.[33] Spin-labeled benzenesulfonamides provided information about the polarity and dynamics of a specific microenvironment within the active site of CA by the ESR analysis.[34] Introduction of the transition metal complex to the parent benzenesulfonamides showed (1) very enhanced inhibitory properties,[35−37] (2) reversible photochemical regulation of CA activity by structural change of the inhibitor,[38] and (3) catalytic inactivation of CA by oxidation of the active site residue.[39] Along this line, ^{129}Xe containing cryptophane molecules acted as nuclear magnetic resonance biosensors targeting CA isozymes.[40] Recently, Hamachi et al. reported supramolecular organic nanoparticles to detect CA by ^{19}F-based magnetic resonance imaging in living cells.[41]

In order to elucidate the complicated mechanisms of photoinduced reactions within metalloprotein matrixes, we newly construct a CA−inhibitor complex by using a benzenesulfonamide group and a wire molecule. In this study, we prepare ruthenium(II) complex-based CA inhibitor, $[Ru(bpy)_2(bpybs)]^{2+}$ {bpy = 2,2′-bipyridine and bpybs = 4′-methyl-2,2′-bipyridinyl-4-carboxylic acid(2-{2-[(4-sulphamoylbenzoylamino)ethoxy]ethoxy}ethyl)amide}, as shown in Scheme 1. The obtained CA−$[Ru(bpy)_2(bpybs)]^{2+}$ complex

Scheme 1. Synthetic Routes of $[Ru(bpy)_2(bpybs)](PF_6)_2$[a]

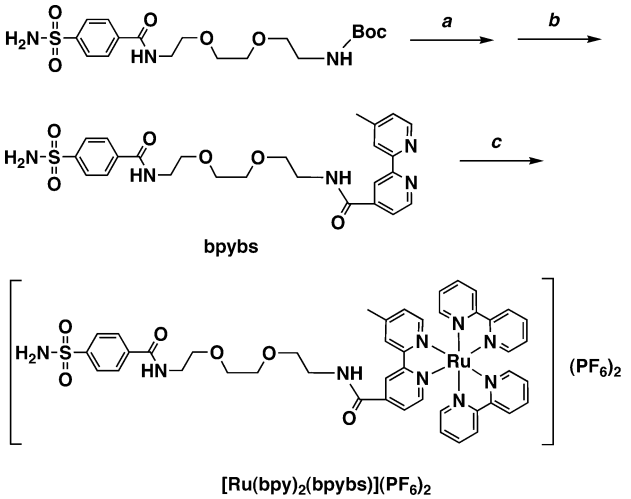

[a]Reagents and conditions: (*a*) TFA, CH_2Cl_2, r.t., 24 h. (*b*) 4′-methyl-2,2′-bipyridinyl-4-carboxylic acid, BOP, DIEA, DMF, r.t., 24 h. (*c*) *cis*-$[RuCl_2(bpy)_2]$, $NaPF_6$, EtOH, 70 °C, 21 h.

possesses one coordinating sulfonamide group to Zn^{2+} ion via an alkyl linkage and one ruthenium(II) complex as a photosensitizer at the surface of CA. This system demonstrates intramolecular or intermolecular photoinduced ET reaction from the excited triplet state of $^3([Ru(bpy)_2(bpybs)]^{2+})^*$ in the presence of an external electron acceptor, such as pentaamminechlorocobalt(III) ($[CoCl(NH_3)_5]^{2+}$) complex. By using preferential metalloenzyme−inhibitor interactions in an aqueous solution, we study the photophysical property of an artificial CA−$[Ru(bpy)_2(bpybs)]^{2+}$ complex, and the detailed ET mechanisms are discussed to regulate the catalytic activity of CA.

RESULTS AND DISCUSSION

Synthesis and Characterization of $[Ru(bpy)_2(bpybs)]Cl_2$ Complex. The synthetic pathway of the ruthenium(II) complex, $[Ru(bpy)_2(bpybs)](PF_6)_2$, was developed according to the literature (Scheme 1).[24] In this study, we used (2-{2-[(4-sulphamoylbenzoylamino)ethoxy]ethoxy}ethyl)carbamic acid *t*-butylester as a starting material.[36c] After deprotecting the Boc group by TFA, the remaining amino group was reacted with the carboxylic group of 4′-methyl-2,2′-bipyridinyl-4-carboxylic acid in the presence of BOP in DMF. Next, the obtained bpybs ligand was combined with a ruthenium(II) complex, *cis*-$[RuCl_2(bpy)_2]$, and then treated with saturated $NaPF_6$ aqueous solution. The red precipitate was collected by filtration, and the desired ruthenium(II) complex, $[Ru(bpy)_2(bpybs)](PF_6)_2$, was obtained. The ^1H NMR, ESI-MS, and UV−vis spectra and elemental analysis clearly support the formation of these compounds, and all signals were reasonably assigned (see the Experimental Section).

The absorption spectrum of the Cl^- form of the ruthenium(II) complex, $[Ru(bpy)_2(bpybs)]Cl_2$, in an aqueous solution shows a broad MLCT band at 458 nm (Table 1). Peak shape

Table 1. Photophysical Properties of the Ruthenium(II) Complexes in N_2-Saturated Aqueous Solution (50 mM HEPES, pH 7.2)[a]

	λ_{max} (nm) (ε (10^4 M^{-1} cm^{-1}))	λ_{em}[b] (nm)	τ (ns) (χ^2)[c]
$[Ru(bpy)_3]Cl_2 \cdot 6H_2O$	452 (1.45)	609	600 (1.01)
$[Ru(bpy)_2(bpybs)](PF_6)_2$	458 (1.31)	652	420 (1.02)

[a]See Figures S1 and S2 in the Supporting Information and ref 42. [b]Excited at 462 nm. [c]Determined by $I_t = A \exp(-t/\tau)$.

and intensity (ε value at absorption maximum) of this spectrum are similar to those of original $[Ru(bpy)_3]Cl_2$ in water (λ_{max} = 452 nm), except for the 6 nm red-shifted λ_{max} of the MLCT, indicating the successful complexation of a ruthenium(II) by the bpybs moiety (Figure S1, Supporting Information).[42] Also, as given in Table 1 and Figure S1 (Supporting Information), photoexcitation of $[Ru(bpy)_2(bpybs)]^{2+}$ (λ_{ex} = 462 nm) provides a strong emission from the excited triplet state of $^3([Ru(bpy)_2(bpybs)]^{2+})^*$ around 652 nm. Compared to the $[Ru(bpy)_3]Cl_2$ complex (λ_{em} = 609 nm), a large red-shift and decrease in the emission intensity are observed probably due to the electron-withdrawing groups at the 4,4′-position of the bpybs ligand. Next, the time-resolved emission decay profile of the excited triplet state of the $[Ru(bpy)_2(bpybs)]^{2+}$ under anaerobic conditions was shown in Figure S2 (Supporting Information). The decay profile was analyzed as a single exponential using the emission intensity (I_t), time (t), lifetime (τ), and the fractional contribution (A) by the following equation.

$$I_t = A \exp(-t/\tau) \quad (1)$$

The emission lifetime was determined to be 0.42 μs (χ^2 = 1.02) for $[Ru(bpy)_2(bpybs)]^{2+}$, whereas a longer lifetime of 0.60 μs (χ^2 = 1.01) was determined for $[Ru(bpy)_3]Cl_2$, as expected due to their emission intensities (Table 1).[42]

dx.doi.org/10.1021/jp310604w | J. Phys. Chem. B 2013, 117, 2625−2635

We next examined the electrochemical property of $[Ru(bpy)_2(bpybs)]^{2+}$ by cyclic voltammetry (CV). The reversible one-electron oxidation wave was presented at +1.38 V (vs $Ag/AgClO_4$) in 0.050 M $[Bu_4N]ClO_4$ acetonitrile solution ($[Ru^{III}(bpy)_2(bpybs)]^{3+}/[Ru^{II}(bpy)_2(bpybs)]^{2+}$; see Table 2)

Table 2. Electrochemical Data of the Ruthenium(II) Complexes in N_2-Saturated Acetonitrile Solution (0.050 M $[Bu_4N]ClO_4$)

	$E_{1/2}{}^a$ (V)		$E_{1/2}{}^a$ (V)	
$[Ru(bpy)_3]Cl_2 \cdot 6H_2O$	+1.38	−1.25	−1.50	−1.74
$[Ru(bpy)_2(bpybs)](PF_6)_2$	+1.38	−1.30	−1.50	−1.74

[a] Against $Ag/AgClO_4$ electrode.

calibrated by 1,1′-dimethyl-4,4′-bipyridinediylium perchlorate, $[MV](ClO_4)_2$ (−0.45 V vs NHE).[43] For the reduction of the bpy ligand, three peaks appeared at −1.25, −1.50, and −1.74 V (vs $Ag/AgClO_4$). We noted that similar electrochemical behavior was observed using $[Ru(bpy)_3]Cl_2$ (+1.38, −1.30, −1.50, and −1.74 V; see Table 2). The slightly positive shift of the reduction potential at −1.25 V was due to the modification of the bpy ligand. On the basis of these measurements, the new ruthenium complex, $[Ru(bpy)_2(bpybs)]^{2+}$, can be expected to perform as a good photosensitizer similar to the original one, $[Ru(bpy)_3]^{2+}$.

Inhibition of CA Activity by $[Ru(bpy)_2(bpybs)]Cl_2$ Complex. In the design of the $[Ru(bpy)_2(bpybs)]^{2+}$ complex, benzenesulfonamide, which is a typical inhibitor of CA, was used for targeting the active site of enzyme. Next, the inhibition property of $[Ru(bpy)_2(bpybs)]^{2+}$ for the CA activity was examined by the conventional ester hydrolysis reaction using *p*-nitrophenyl acetate (*p*-NPA) as the substrate.[44,45] The hydrolysis was followed by monitoring the absorbance at 348 nm, and then, the initial rate, v_{ini}, was determined for various substrate concentrations. The CA activity was effectively suppressed by a synthetic $[Ru(bpy)_2(bpybs)]^{2+}$ inhibitor, and its Michaelis−Menten plot is summarized in Figure 1 with a series of typical CA inhibitors, *p*-aminoethylbenzenesulfonamide (*p*-AEBS), *p*-carboxybenzenesulfonamide (*p*-CBS), and *p*-nitrobenzenesulfonamide (*p*-NBS). From these data, we obtained the kinetic parameters, k_{cat} and K_m, for the native CA activity by using the Michaelis−Menten equation:

$$v_{ini} = k_{cat}[E]_0[S]/([S] + K_m) \quad (2)$$

In the presence of several inhibitors, the least-squares curve-fitting analysis with the Michaelis−Menten equation for the competitive inhibition was conducted to estimate the parameter of K_I as follows:

$$v_{ini} = k_{cat}[E]_0[S]/\{K_m(1 + [I]_0/K_I) + [S]\} \quad (3)$$

where k_{cat}, K_m, and K_I represent the first-order rate constant for the catalyst−substrate complex in the presence of inhibitor, the Michaelis−Menten constant, and the dissociation constant between enzyme and inhibitor, respectively. The symbols $[E]_0$, $[I]_0$, and $[S]$ represent the initial concentrations of CA, inhibitor, and substrate, respectively. The calculated parameters are summarized in Table 3. In our experiments, CA showed a catalytic activity having a k_{cat} value of 8.9 ± 0.9 s^{-1} almost comparable with the reported ones.[46] We found that the K_I value between CA and $[Ru(bpy)_2(bpybs)]^{2+}$ inhibitor was determined to be 1.9 ± 0.2 μM. Therefore, this ruthenium complex type of inhibitor can be effective as well as *p*-CBS (K_I = 2.2 ± 0.3 μM), showing an intermediate K_I value between *p*-AEBS (4.1 ± 0.7 μM) and *p*-NBS (0.48 ± 0.05 μM). Recently, Dmochowski et al. reported the X-ray crystal structure of CA with a large cryptophane-type inhibitor containing a benzenesulfonamide group.[40] Its K_I value was determined to be 0.1 μM by isothermal titration calorimetric experiment, which was comparable with those of our system. From molecular structures of the $[Ru(bpy)_2(bpybs)]^{2+}$ and its synthetic cryptophane-type inhibitor, it is indicated that the distances and the conformations of the "wire" moiety in these molecules affect the K_I values between synthetic benzenesulfonamide inhibitor and CA. Also, on the basis of the X-ray structural data of CA, we illustrate the CA−$[Ru(bpy)_2(bpybs)]^{2+}$ complex, including Zn^{2+} ion (yellow), Tyr6 (red), and coordinated His residues, as shown in Figure 2. Since the edge-to-edge distance of the amide linkage of the bpybs ligand is about 20 Å, the bulky ruthenium moiety of the $[Ru(bpy)_2(bpybs)]^{2+}$ complex may locate outside the active site of CA and block the substrate entry.[46−48]

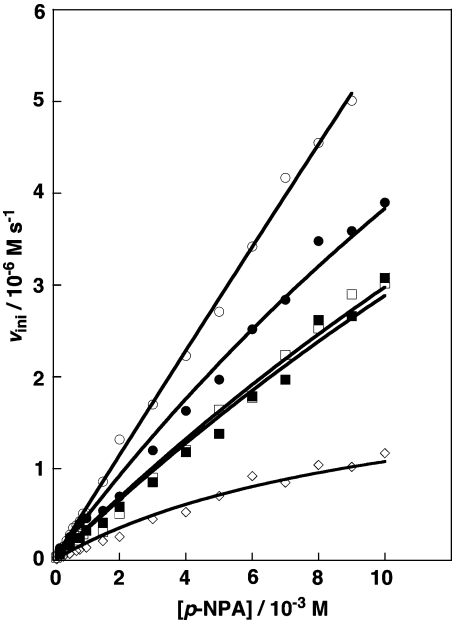

Figure 1. Michaelis−Menten plots for the hydrolysis of *p*-NPA in 50 mM HEPES buffer containing 10% acetonitrile, pH 7.2 and 25 °C ([E] = [I] = 2.0×10^{-6} M, [*p*-NPA] = 2.0×10^{-4} to 1.0×10^{-2} M): (open circles) native CA; (closed circles) *p*-AEBS; (open squares) *p*-CBS; (closed squares) *p*-$[Ru(bpy)_2(bpybs)]^{2+}$; (open diamonds) *p*-NBS. Solid curves are fittings to eq 2 or 3.

Table 3. Kinetic Parameters for CA Activity in the Hydrolysis of *p*-NPA at 25 °C

	k_{cat} (s^{-1})	K_m (10^{-2} s^{-1})	K_I (10^{-6} M)
native CA	8.9 ± 0.9	2.6 ± 0.4	
p-AEBS			4.1 ± 0.7
p-CBS			2.2 ± 0.3
$[Ru(bpy)_2(bpybs)]^{2+}$			1.9 ± 0.2
p-NBS			0.48 ± 0.05

Photoirradiation Effect on the Catalytic Activity. It is well-known that a $[CoCl(NH_3)_5]^{2+}$ complex can be employed as a sacrificial oxidative quencher for the photoexcited state of $^3\{[Ru(bpy)_3]^{2+}\}^*$ in an aqueous solvent, because the one-electron redox potential of $[CoCl(NH_3)_5]^{2+}$ is +0.52 V vs NHE.[8,9,49] Next, we studied CA activity after photoirradiation

dx.doi.org/10.1021/jp310604w | J. Phys. Chem. B 2013, 117, 2625−2635

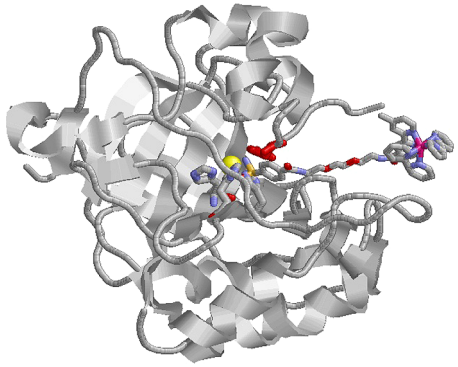

Figure 2. Illustration of the CA–$[Ru(bpy)_2(bpybs)]^{2+}$ complex by using RasWin software, including Zn^{2+} ion (yellow), Tyr6 (red), and coordinated His residues.

of the $[Ru(bpy)_2(bpybs)]^{2+}$ in the presence of $[CoCl(NH_3)_5]^{2+}$. Upon the visible light (λ > 430 nm) irradiation to the N_2-purged aqueous solution (pH 7.2, 50 mM HEPES buffer) containing CA and $[Ru(bpy)_2(bpybs)]^{2+}$ (1:1, 2.0 μM each) with an excess amount of $[CoCl(NH_3)_5]^{2+}$ (10 mM) at 25 °C, the *p*-NPA hydrolysis reaction was followed by UV–vis spectroscopy according to the same procedure. As shown in Figure 3, changes in the absorbance at 348 nm (ΔA_{348})

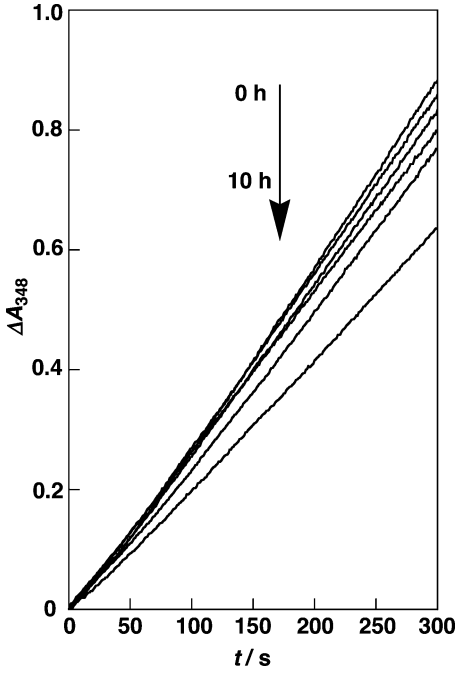

Figure 3. Changes in the absorption at 348 nm for the hydrolysis of *p*-NPA by CA upon photoirradiation (λ > 430 nm) in 50 mM HEPES buffer, pH 7.2 and 25 °C ([CA] = [Ru(II)] = 2.0 μM, [Co(III)] = 10 mM, [*p*-NPA] = 2.0 mM in acetonitrile). Irradiation times are 0, 1, 2, 3, 4, and 10 h, respectively.

gradually decreased with increasing irradiation time (~28% decrease after 10 h). The initial rates of hydrolysis reactions are summarized in Table 4. In the case of the 1:2 mixture of CA with $[Ru(bpy)_2(bpybs)]^{2+}$, the decrease in v_{ini} was greater than that of the 1:1 one, indicating the efficiency for the photoexcitation of the CA–$[Ru(bpy)_2(bpybs)]^{2+}$ complex is important. For this system, we propose the photoinduced ET mechanism, as displayed in Scheme 2. According to the

Table 4. Initial Rates (v_{ini}) for CA Activity in the Hydrolysis of *p*-NPA after Photoirradiation (λ > 430 nm) at Different $[Ru(bpy)_2(bpybs)]^{2+}$ Concentrations[a]

irradiation time (h)	v_{ini}[b] (10^{-7} M s^{-1}) ([Ru] = 2.0 μM)	v_{ini}[b] (10^{-7} M s^{-1}) ([Ru] = 4.0 μM)
0	6.0	4.8
1	5.9	4.7
2	5.9	4.6
3	5.8	4.5
4	5.5	4.1
5	5.1	3.4
10	4.3	2.3

[a][CA] = 2.0 μM, $[CoCl(NH_3)_5^{2+}]$ = 10 mM, and [*p*-NPA] = 2.0 mM in 50 mM HEPES buffer (pH 7.2) containing 10% acetonitrile at 25 °C. [b]The experimental errors are within 7%.

Scheme 2. Photoinduced ET Reactions between CA–$[Ru(bpy)_2(bpybs)]^{2+}$ Complex and $[CoCl(NH_3)_5]^{2+}$

$$CA + [Ru(bpy)_2(bpybs)]^{2+} \underset{K_I}{\rightleftharpoons} CA\text{-}[Ru(bpy)_2(bpybs)]^{2+}$$

$$CA\text{-}[Ru(bpy)_2(bpybs)]^{2+} \underset{k_0}{\overset{h\nu}{\rightleftharpoons}} CA\text{-}^3\{[Ru(bpy)_2(bpybs)]^{2+}\}^*$$

$$CA\text{-}^3\{[Ru(bpy)_2(bpybs)]^{2+}\}^* + [CoCl(NH_3)_5]^{2+} \xrightarrow{k_q} CA\text{-}[Ru(bpy)_2(bpybs)]^{3+} + [Co(H_2O)_6]^{2+} + Cl^- + 5NH_4^+$$

$$CA\text{-}[Ru(bpy)_2(bpybs)]^{3+} \xrightarrow{k_{IET}} {}^{\bullet+}CA\text{-}[Ru(bpy)_2(bpybs)]^{2+}$$

dissociation constant for the CA–$[Ru(bpy)_2(bpybs)]^{2+}$ complex, over 83% of the CA–inhibitor complex was formed under our photophysical measurement conditions. The initial ET quenching reaction between the photoexcited state of CA–$^3([Ru(bpy)_2(bpybs)]^{2+})^*$ and $[CoCl(NH_3)_5]^{2+}$ gives CA–$[Ru(bpy)_2(bpybs)]^{3+}$. Since $[Ru(bpy)_2(bpybs)]^{3+}$ is a powerful oxidant (+1.38 V), as observed in the CV experiment, the following intramolecular ET from an amino-acid residue near the active site of CA to $[Ru(bpy)_2(bpybs)]^{3+}$ is thermodynamically favorable. The resulting oxidized CA radical cation, $CA^{\bullet+}$, may be unstable. Therefore, the final product of $CA^{\bullet+}$ is still unclear at this stage, due to the difficulties of isolation of the oxidized protein and its characterization. As previously described by Cowan et al. using a metallopeptide–sulfonamide conjugate,[39] the oxidized CA is catalytically inactive and the steady-state photoirradiation of the CA–$[Ru(bpy)_2(bpybs)]^{2+}$–$[CoCl(NH_3)_5]^{2+}$ system for a long time may generate such inactive CA.

In our system, the intermolecular electron-trasfer reaction from $^3\{[Ru(bpy)_3]^{2+}\}^*$ to $[CoCl(NH_3)_5]^{2+}$ gives $[Co(H_2O)_6]^{2+}$. This process is irreversible and prevents the charge recombination reaction (Scheme 2). In the photoirradiation experiment, we also tried to use another oxidation agent, hexaammineruthenium(III) ($[Ru(NH_3)_6]^{3+}$), instead of $[CoCl(NH_3)_5]^{2+}$ under the same conditions. Such a control experiment did not show the inhibition effect of CA activity (data not shown), probably because the electron transfer is reversible. The efficiency of the CA inhibition by photoirradiation would not be enough, but the use of a sacrificial acceptor $[CoCl(NH_3)_5]^{2+}$ is essential at this stage.

dx.doi.org/10.1021/jp310604w | J. Phys. Chem. B 2013, 117, 2625–2635

To confirm the importance of an intramolecular ET process within the CA−$[Ru(bpy)_2(bpybs)]^{2+}$ complex, we next conducted a control experiment by using an intermolecular system, such as an equimolar mixture of $[Ru(bpy)_3]^{2+}$, *p*-CBS, and CA (2.0 μM each) in the presence of $[CoCl(NH_3)_5]^{2+}$ (10 mM). As shown in Figure S3 (Supporting Information), there was no effect on the hydrolysis reaction by light irradiation, indicating CA possesses native catalytic activity even after photoirradiation. The intermolecular photoinduced ET reaction between CA and the photo-oxidized $[Ru(bpy)_3]^{3+}$ did not proceed. Therefore, it is obvious that the methylene wire linkage between the benzenesulfonamide group and the bpy ligand of the $[Ru(bpy)_2(bpybs)]^{2+}$ is essential for photo-oxidation of CA by making the CA−$[Ru(bpy)_2(bpybs)]^{2+}$ complex.

Emission Lifetime and Transient Absorption Studies. To investigate the reaction kinetics in detail, we next conducted lifetime and laser flash photolysis experiments. Figure 4 displays

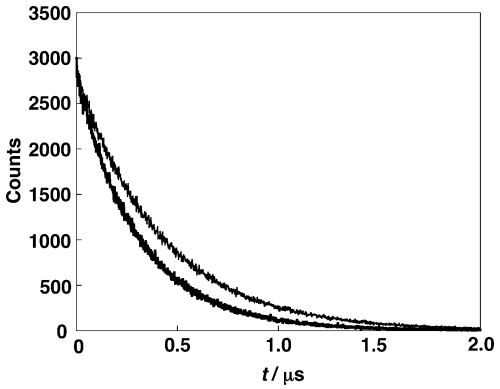

Figure 4. Emission decay for the $[Ru(bpy)_2(bpybs)]^{2+}$−CA system (50 μM, each) in the absence (normal line) and the presence of 10 mM $[CoCl(NH_3)_5]^{2+}$ (bold line), measured with the excitation wavelength λ_{ex} = 450 nm in a N_2-saturated 50 mM HEPES buffer at pH 7.2 and 25 °C.

emission decay of the excited $^3([Ru(bpy)_2(bpybs)]^{2+})^*$ in the absence and the presence of CA and $[CoCl(NH_3)_5]^{2+}$, measured with the excitation wavelength λ_{ex} = 450 nm in a N_2-saturated 50 mM HEPES buffer at pH 7.2 and 25 °C. The lifetimes, τ, after photoirradiation of $[Ru(bpy)_2(bpybs)]^{2+}$, a 1:1 mixture of $[Ru(bpy)_2(bpybs)]^{2+}$ with CA (10 μM, each), and the mixture of $[Ru(bpy)_2(bpybs)]^{2+}$ and CA (10 μM, each) with $[CoCl(NH_3)_5]^{2+}$ were estimated as shown in Table 5. The $^3([Ru(bpy)_2(bpybs)]^{2+})^*$ has a lifetime of τ_0 = 0.42 μs (χ^2 = 1.06) analyzed as a single exponential using eq 1. A similar lifetime of τ = 0.44 μs (χ^2 = 1.03) for the CA−$[Ru(bpy)_2(bpybs)]^{2+}$ complex was obtained, although τ = 0.31 μs (χ^2 = 1.12) was found in the case of the CA−$[Ru(bpy)_2(bpybs)]^{2+}$−$[CoCl(NH_3)_5]^{2+}$ system. These results clearly support the oxidative quenching by a $[CoCl(NH_3)_5]^{2+}$ ion.

Table 5. Lifetimes (τ) after Photoirradiation of $[Ru(bpy)_2(bpybs)]^{2+}$−CA Complex in the Absence and Presence of $[CoCl(NH_3)_5]^{2+}$ Monitored by Emission and Transient Absorption Measurements

	emission	transient absorption	
complexes	τ (μs)	τ (μs) (375 nm)	τ (μs) (450 nm)
$[Ru(bpy)_2(bpybs)]^{2+}$−CA	0.44	0.50	0.50
$[Ru(bpy)_2(bpybs)]^{2+}$−CA + $[CoCl(NH_3)_5]^{2+}$	0.31	0.40	0.40 (84%), 15 (19%)

Next, transient absorption spectra of CA−$[Ru(bpy)_2(bpybs)]^{2+}$ complex (50 μM, each) in a degassed 50 mM HEPES buffer at pH 7.2 and 25 °C were monitored after the flash photoirradiation (Figure 5a). In the 0.1−10 μs range

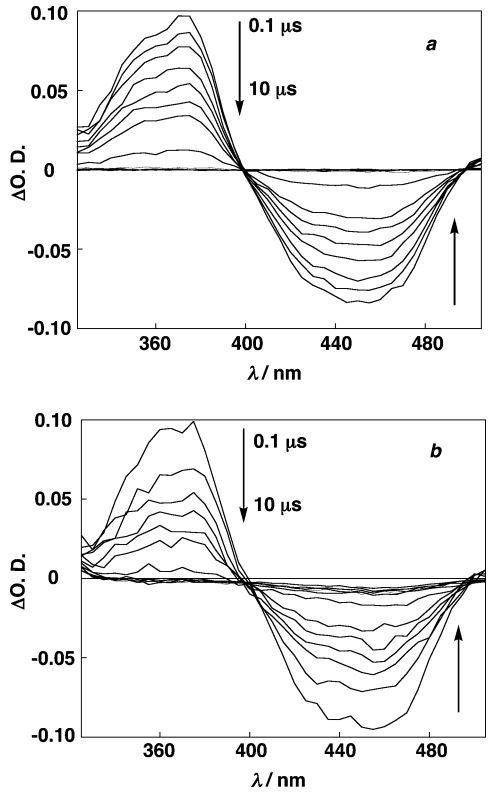

Figure 5. Transient absorption spectra for the $[Ru(bpy)_2(bpybs)]^{2+}$−CA system (50 μM, each) (a) in the absence and (b) the presence of $[CoCl(NH_3)_5]^{2+}$ (10 mM) after irradiation by the 532 nm laser in a degassed 50 mM HEPES buffer at pH 7.2 and 25 °C, respectively. Spectra were recorded at 0.1, 0.2, 0.3, 0.4, 0.5, 1.0, 2.0, 3.0, 4.0., 5.0, and 10 μs.

after laser pulses, a decay of the excited triplet state of $^3([Ru(bpy)_2(bpybs)]^{2+})^*$ and a recovery of the ground state were detected around 375 and 450 nm of the MLCT band region, respectively, with an isosbestic point at 400 nm. The ΔO.D. for the time course of absorbance at 375 and 450 nm reached zero within 5.0 μs (Figure 6a) and also gave a single-exponential curve having a lifetime of τ_0 = 0.50 μs. In case of the CA−$[Ru(bpy)_2(bpybs)]^{2+}$−$[CoCl(NH_3)_5]^{2+}$ system, the $^3([Ru(bpy)_2(bpybs)]^{2+})^*$ signal around 375 nm appeared (τ = 0.40 μs), but the recovery of a MLCT bleaching at 450 nm without an isosbestic point at 400 nm was different from that of the $[Ru(bpy)_2(bpybs)]$−CA system (Figure 5b). As shown in Figure 6b, the time course absorbance change at 450 nm suggests the biphasic kinetics. The first step is a fast reaction, reaching completion within 1 μs after laser photolysis. The reaction of the second step is slower in the time range 1−80 μs (inset of Figure 6b). Therefore, we estimate the fast component of τ_1 and the slower one τ_2 as 0.40 μs (81%) and 15 μs (19%), respectively. The photoinduced ET mechanism is described in Scheme 2. The photoexcited $^3([Ru(bpy)_2(bpybs)]^{2+})^*$ is oxidatively quenched by $[CoCl(NH_3)_5]^{2+}$ to give [Ru-

dx.doi.org/10.1021/jp310604w | J. Phys. Chem. B 2013, 117, 2625−2635

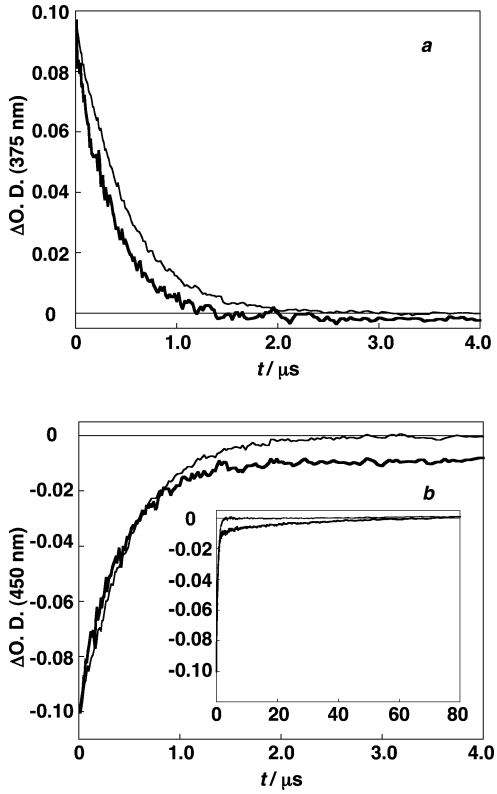

Figure 6. Absorption changes for the $[Ru(bpy)_2(bpybs)]^{2+}$–CA system (50 μM, each) monitored at (a) 375 nm and (b) 450 nm in the absence (normal line) and the presence of 10 mM $[CoCl(NH_3)_5]^{2+}$ (bold line) after irradiation by the 532 nm laser in a degassed 50 mM HEPES buffer at pH 7.2 and 25 °C, respectively. The inset of part b provides from 0 to 80 μs.

$(bpy)_2(bpybs)]^{3+}$. When a 10 mM concentration of $[CoCl(NH_3)_5]^{2+}$ is used under our experimental conditions, the second-order rate constant, k_q, for the initial step is calculated to be 4.8×10^7 M^{-1} s^{-1} (τ_1 = 0.40 μs). Then, the oxidized $[Ru(bpy)_2(bpybs)]^{3+}$ complex abstracts an electron from CA. The first-order rate constant for this second step, k_{IET}, is also determined to be 6.6×10^4 s^{-1} (τ_1 = 15 μs) from the slower component (19%) in Figure 6b.

It is known that there are some models on the intramolecular ET reactions from an amino acid residue of Tyr or tryptophan (Trp) to photogenerated $[Ru(bpy)_3]^{3+}$.[50] According to the X-ray crystal structure of bovine CA, one of the amino acid candidates for the intramolecular ET is tyrosine (Tyr6) nearby the enzyme active site.[29,30] The other Tyr/Trp residues in CA are far from $[Ru(bpy)_3]^{3+}$ compared to Tyr6. The driving force, $\Delta G°$, for the ET reaction from Tyr6 to Ru(III) is estimated to be $\Delta G° = -0.33$ eV at pH 7 from the difference of the standard potentials between $[Ru(bpy)_3]^{3+}/[Ru(bpy)_3]^{2+}$ (1.26 V vs NHE) and $TyrO^{\bullet+}$/TyrOH (0.93 V vs NHE).[50a,b] In the case of the covalently linked $[Ru(bpy)_3]^{2+}$–Tyr conjugate systems, an electron acceptor such as methylviologen (MV^{2+}) or $[Ru(NH_3)_6]^{3+}$ was added. A laser flash excited the $[Ru(bpy)_3]^{2+}$ moiety that was rapidly oxidized to Ru(III) by this external acceptor.[51] The intramolecular ET could then be followed using the subsequent transient absorption changes of the Ru(II) recovery at 450 nm and the generation of the $Tyr^{\bullet+}$ radical cation at 410 nm. Thus, they successfully gave the first-order rate constant, $k = 10^5$ s^{-1}, for the intramolecular ET at pH 7.0, which was comparable with that of k_{IET} in our system.

The $[CoCl(NH_3)_5]^{2+}$ ion is the sacrificial electron acceptor, and therefore, the charge separated state after the photoinduced ET reactions, the reduced Co(II) and $Tyr^{\bullet+}$ radical cation, can be formed. The estimated distance between Tyr6 and $[Ru(bpy)_3]^{3+}$ (~20 Å) is favorable for the intramolecular electron-transfer reaction within the CA–$[Ru(bpy)_2(bpybs)]^{2+}$ complex. However, in our present experimental conditions, the oxidized $Tyr^{\bullet+}$ radical cation could not be clearly detected by transient absorption (Figure 5b), mainly due to the small absorption coefficient at 410 nm ($\varepsilon_{410} = 2.75 \times 10^3$ M^{-1} cm^{-1}).[52]

In order to monitor the charge separated state by transient absorption spectra, we further used MV^{2+} instead of $[CoCl(NH_3)_5]^{2+}$ as an initial electron acceptor. Figure 7a shows the

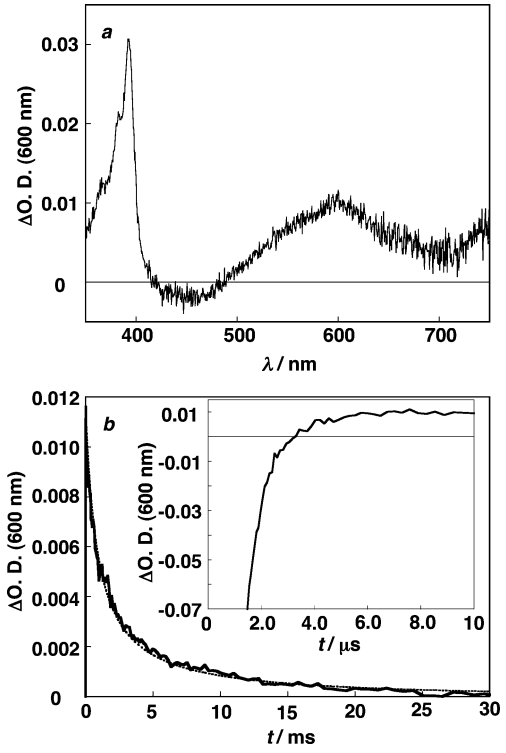

Figure 7. (a) Transient absorption spectrum for the $[Ru(bpy)_2(bpybs)]^{2+}$–CA system (50 μM, each) in the presence of 5.0 mM MV^{2+} after irradiation by the 480 nm laser in a degassed 50 mM HEPES buffer at pH 7.2 and 25 °C. The spectrum was recorded at 14 μs. (b) Absorption change for the decay of the $MV^{\bullet+}$ radical cation monitored at 600 nm. The dotted curve is a fitting to eq 4. The inset provides from 0 to 10 μs for the formation of the $MV^{\bullet+}$ radical cation.

transient absorption spectrum obtained after 14 μs of laser irradiation of the excited $^3([Ru(bpy)_2(bpybs)]^{2+})^*$ in the presence of CA (50 μM, each) and MV^{2+} (5 mM), measured at 600 nm with the excitation wavelength λ_{ex} = 480 nm in a degassed 50 mM HEPES buffer at pH 7.2 and 25 °C. The shape and intensities of the obtained spectrum are almost identical to the $MV^{\bullet+}$ radical cation.[43a] Although a small absorption due to the oxidized $Tyr^{\bullet+}$ was not obtained in the same kinetics, we successfully observed the transient absorption change for the formation (inset of Figure 7b) and the decay (Figure 7b) of a viologen radical cation ($MV^{\bullet+}$) at 600 nm having a longer lifetime. This process suggests the bimolecular charge recombination between $MV^{\bullet+}$ and $CA^{\bullet+}$, as depicted in Scheme 3. That is, the $[Ru(bpy)_2(bpybs)]^{2+}$ ground state

dx.doi.org/10.1021/jp310604w | J. Phys. Chem. B 2013, 117, 2625–2635

Scheme 3. Photoinduced ET Reactions between CA–$[Ru(bpy)_2(bpybs)]^{2+}$ Complex and MV^{2+}

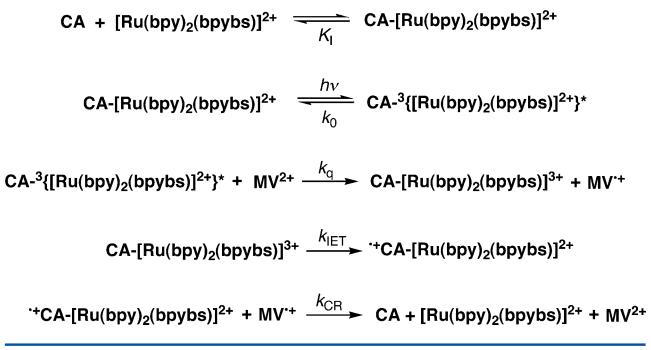

recovery monitored at 450 nm was faster (~10 μs) due to the intramolecular electron transfer from CA to the photooxidized Ru(III) inhibitor, followed by the charge recombination of $MV^{\bullet+}$ with $CA^{\bullet+}$. Thus, the second-order rate constant of the thermal charge recombination reaction (k_{CR}) was evaluated from the decay of $MV^{\bullet+}$ at 600 nm after the quenching of $^3([Ru(bpy)_2(bpybs)]^{2+})^*$ was completed (eq 4):

$$A_t = (A_0 + k_b[A]_0 A_\infty t)/(1 + k_b[A]_0 t) \quad (4)$$

Here, A_0, A_t, and A_∞ are the ΔO.D. values at time 0, t, and infinity, respectively, and $[A]_0$ is the initial concentration of $MV^{\bullet+}$. Three unknown parameters, A_0, $k[A]_0$, and A_∞, were simultaneously estimated. By using the value of $[A]_0$ calculated from the concentration of $MV^{\bullet+}$ (ε_{600} = 1.30 × 10^4 M^{-1} cm^{-1}),[43a] k_{CR} was then determined as k_{CR} = 1.2 × 10^9 M^{-1} s^{-1}. We also note that absorption decay of the $MV^{\bullet+}$ radical cation, generated by photoirradiation of the bimolecular $[Ru(bpy)_2(bpybs)]^{2+}$ and MV^{2+} system in the absence of CA, was completed within 5 ms (data not shown) and much faster than that of the $[Ru(bpy)_2(bpybs)]^{2+}$–CA–MV^{2+} one. Therefore, we produced a multistep photoinduced ET triad comprising a $[Ru(bpy)_2(bpybs)]^{2+}$–CA and an electron acceptor, such as $[CoCl(NH_3)_5]^{2+}$ or MV^{2+}. Our experiments also indicated that both intermolecular and intramolecular photoinduced ET reactions are the essential events to regulate the CA enzyme activity. Finally, the present model system based on a CA and $Ru(bpy)_3$ wire complex is one of the new interesting biomimetic models for the intramolecular photoinduced ET reactions within a protein scaffold.

CONCLUSIONS

In conclusion, we have prepared a ruthenium(II)-based CA inhibitor, $[Ru(bpy)_2(bpybs)]^{2+}$, tethering a benzenesulfonamide group and a $[Ru(bpy)_3]^{2+}$ moiety and constructed the artificial CA–Ru(II) complex. The CA activity was effectively suppressed by a synthetic $[Ru(bpy)_2(bpybs)]^{2+}$ inhibitor. The dissociation constant, K_I, for the $[Ru(bpy)_2(bpybs)]^{2+}$ inhibitor at pH 7.2 and at 25 °C is comparable with those of the commercially available ones, that is, the order of K_I is *p*-AEBS > *p*-CBS ≈ $[Ru(bpy)_2(bpybs)]^{2+}$ > *p*-NBS. After steady-state photoirradiation, the photoexcited triplet state of $^3([Ru(bpy)_2(bpybs)]^{2+})^*$ was quenched by a sacrificial quencher through an intermolecular photoinduced ET mechanism, giving the oxidized $[Ru(bpy)_2(bpybs)]^{3+}$. Then, the following intramolecular electron abstraction from an amino-acid residue near the active site of CA proceeded and the resulting oxidized CA was catalytically inactive. These results revealed that the intramolecular ET is the important process to regulate CA activity by the visible light irradiation in our system. Finally, we discussed the reaction kinetics in detail by emission lifetime and transient absorption measurements. Both the second-order rate constant for the initial step and the first-order rate constant for the second step were determined, and the latter of which was similar to those of the previously reported model dyads. Clear formation of the long-lived viologen radical cation suggested that the intramolecular electron abstraction from CA by the oxidized $[Ru(bpy)_2(bpybs)]^{3+}$ is a crucial event. We believe further synthetic manipulations on the $[Ru(bpy)_3]^{2+}$ wire molecules that bind to the CA active site may provide valuable information to elucidate the mechanism of the biological photoinduced ET reactions within artificial CA–inhibitor complexes and insights into applications to design of the metal complex-based enzyme inhibitor in the biological systems.

EXPERIMENTAL SECTION

Materials. Benzotriazol-1-yloxytris(dimethylamino)-phosphonium hexafluorophosphate (BOP), diisopropylethylamine (DIEA), *N*,*N*-dimethylformamide (DMF), trifluoroacetic acid (TFA), *p*-aminoethylbenzenesulfonamide (*p*-AEBS), *p*-carboxybenzenesulfonamide (*p*-CBS), *p*-nitrobenzenesulfonamide (*p*-NBS), ethanol, and $NaPF_6$ were purchased from Wako Chemicals and used as received. *cis*-(2,2′-Bipyridine)-dichlororuthenium(II) dihydrate ($[RuCl_2(bpy)_2]\cdot 2H_2O$), tris-(2,2′-bipyridine)ruthenium(II) dichloride hexahydrate ($[Ru(bpy)_3]Cl_2\cdot 6H_2O$), pentaamminechlorocobalt(III) dichloride ($[CoCl(NH_3)_5]Cl_2$), *p*-nitrophenylacetate (*p*-NPA), and carbonic anhydrase from bovine (CA) were obtained from Aldrich. 4-(2-Hydroxyethyl)-1-piperazineethanesulfonic acid (HEPES) and tetra-*n*-butylammonium perchlorate ($[Bu_4N]ClO_4$) were purchased from Tokyo Kasei Co. and Fluka, respectively. 4′-Methyl-2,2′-bipyridinyl-4-carboxylic acid and (2-{2-[(4-sulphamoylbenzoylamino)ethoxy]ethoxy}ethyl)-carbamic acid *t*-butylester were prepared according to the literature methods.[36c,53] Column chromatography on silica gel was carried out by using Silicagel 60 (Kanto Chemical Co.). All other reagents and solvents were of guaranteed grade. All aqueous solutions were prepared from redistilled water.

Synthesis of bis(2,2′-Bipyridine){4′-methyl-2,2′-bipyridinyl-4-carboxylic acid(2-{2-[(4-sulphamoylbenzoylamino)ethoxy]ethoxy}ethyl)amide} Ruthenium(II) Hexafluorophosphate {$[Ru(bpy)_2(bpybs)](PF_6)_2$}. *Synthesis of 4′-Methyl-2,2′-bipyridinyl-4-carboxylic acid(2-{2-[(4-sulphamoylbenzoylamino)ethoxy]ethoxy}ethyl)amide (bpybs).* (2-{2-[(4-Sulphamoylbenzoylamino)ethoxy]ethoxy}ethyl)-carbamic acid *t*-butylester (0.29 g, 6.7 × 10^{-4} mol) was dissolved in 25 mL of CH_2Cl_2 and then reacted with TFA (4.0 mL, 5.3 × 10^{-2} mol) for 24 h at room temperature. After removal of the solvent and unreacted TFA by evaporation several times, the residue was then used for the next step. Next, to a solution of the remaining amino compound in 15 mL of DMF, DIEA (0.25 mL, 1.5 × 10^{-3} mol) and BOP (0.60 g, 1.3 × 10^{-3} mol) in 5 mL of DMF were added and stirred at room temperature for 2 h. Then, 20 mL of a solution of 4′-methyl-2,2′-bipyridinyl-4-carboxylic acid (0.46 g, 2.2 × 10^{-3} mol) in DMF was added dropwise and reacted for 24 h at room temperature. After removal of the solvent in vacuo, the crude mixture was dissolved in 30 mL of CH_2Cl_2. The solution was washed with 30 mL of saturated NaCl(aq) four times, and the organic layer was dried over Na_2SO_4. The solvent was evaporated to dryness, and the residue was subjected to a

dx.doi.org/10.1021/jp310604w | J. Phys. Chem. B 2013, 117, 2625–2635

flash column chromatography on silica gel (ϕ 2.5 cm × 20 cm, CH_2Cl_2–MeOH = 100:1–90:1 (v/v)). A pale yellow band was collected and was evaporated to yield the desired compound, 0.16 g (44%). ESI-MS (MeOH, m/z) 550.21 ($[M+Na]^+$ requires 550.58). ^{1}H NMR (400 MHz, CD_3OD, 298 K, TMS): δ/ppm = 2.49 (s, 3H, methyl), 3.19–3.27 (m, 4H, $-OCH_2CH_2O-$), 3.46–3.48 (m, 4H, $-OCH_2CH_2NH-$), 3.53–3.65 (m, 4H, $-NHCH_2CH_2O-$), 7.32 (d, 1H, J = 4.8 Hz, bpy-5H), 7.75 (d, 1H, J = 5.0 Hz, bpy-5′H), 7.87–7.94 (m, 4H, Ar–H in benzene), 8.21 (s, 1H, bpy-3H), 8.52 (d, 1H, J = 5.0 Hz, bpy-6H), 8.64 (s, 1H, bpy-3′H), 8.75 (d, 1H, J = 5.0 Hz, bpy-6′H). Anal. Calcd for $C_{25}H_{29}N_5O_6S{\cdot}CH_3OH{\cdot}0.5CH_2Cl_2$: C, 52.86; H, 5.69; N, 11.63%. Found: C, 52.22; H, 5.45; N, 11.22%.

Preparation of bis(2,2′-Bipyridine){4′-methyl-2,2′-bipyridinyl-4-carboxylic acid(2-{2-[(4-sulphamoylbenzoylamino)-ethoxy]ethoxy}ethyl)amide} Ruthenium(II) Hexafluorophosphate {[Ru(bpy)$_2$(bpybs)](PF$_6$)$_2$}. To a solution of *cis*-$[RuCl_2(bpy)_2]{\cdot}2H_2O$ (44 mg, 9.1 × 10^{-5} mol) in 120 mL of ethanol, bpybs (96 mg, 1.8 × 10^{-4} mol) in 25 mL of ethanol was added and refluxed at 70 °C for 21 h. After cooling down to room temperature, the solvent was removed on a rotary evaporator. The residue was dissolved in water and then reprecipitated by adding saturated $NaPF_6$ aqueous solution. The red precipitate was collected by filtration. This was washed with water, and the product (0.049 g) was obtained in 44% yield. ESI-MS (MeOH, m/z) 940.33 ($[M-(PF_6)_2-H]^+$ requires 940.02), 1086.34 ($[M-PF_6]^+$ requires 1086.00). ^{1}H NMR (400 MHz, CD_3OD, 298 K, TMS): δ/ppm = 2.96 (s, 3H, methyl), 3.64–3.70 (m, 12H, $-CH_2CH_2-$), 7.34 (d, 1H, J = 6.0 Hz, bpy-5H), 7.44–7.50 (m, 4H, bpy-6H), 7.61 (d, 1H, J = 5.8 Hz, bpy-6H), 7.72 (d, 1H, J = 6.0 Hz, bpy-5H), 7.78–7.82 (m, 4H, bpy-5H), 7.84 (s, 4H, Ar–H in benzene), 7.91 (d, 1H, J = 6.0 Hz, bpy-6H), 8.07–8.14 (m, 4H, bpy-4H), 8.59 (s, 1H, bpy-3H), 8.66–8.70 (m, 4H, bpy-3H), 8.96 (s, 1H, bpy-3H). UV–vis (water, λ/nm) 458 (MLCT band, ε = 1.31 × 10^4 M^{-1} cm^{-1}). Anal. Calcd for $C_{45}H_{45}N_9O_6P_2F_{12}RuS$: C, 43.60; H, 4.02; N, 9.99%. Found: C, 43.91; H, 3.68; N, 10.24%. To conduct the spectroscopic measurements in an aqueous solution, the counteranions of $[Ru(bpy)_2(bpybs)](PF_6)_2$ were converted to the Cl^- form. The $[Ru(bpy)_2(bpybs)](PF_6)_2$ was dissolved in 10 mL of MeOH, and column chromatography on Dowex1-X8 (Cl^- form, ϕ 2.5 cm × 20 cm, MeOH) afforded $[Ru(bpy)_2(bpybs)]Cl_2$.

Enzymatic Activity Experiment. The hydrolytic activity of CA was studied on an UV–vis spectrophotometer with a Shimadzu UV-2550 instrument at 25 °C in 50 mM HEPES buffer (pH 7.2) containing 10% acetonitrile. Initial rates of *p*-nitrophenyl acetate hydrolysis were determined by the increase of the absorbance at 348 nm ($\Delta\varepsilon$ = 5.00 × 10^3 M^{-1} cm^{-1}) for the release of *p*-nitrophenolate as a product.[44,45] The concentration of CA was determined by absorbance at 280 nm using the molar extinction coefficient of ε = 5.00 × 10^4 M^{-1} cm^{-1}.[50] Substrate concentrations were varied from 0.2 to 10 mM, and initial rates were plotted against substrate concentrations. The stock solution of *p*-nitrophenyl acetate (10, 100, and 150 mM) were prepared with acetonitrile. Kinetic parameters were obtained by the least-squares curve-fitting analysis with the Michaelis–Menten equation using Kaleida Graph Software (Synergy Software).

Photoreaction Measurements. Sample solutions were purged with N_2 gas for 20 min before the photoreaction experiments. The stock solution of $[Ru(bpy)_2(bpybs)]Cl_2$ was mixed with CA and $[Co(NH_3)_5Cl]Cl_2$ dissolved in 50 mM HEPES buffer (pH 7.2). The final concentrations of CA and $[Co(NH_3)_5Cl]Cl_2$ were constant at 2.0 × 10^{-6} M and 10 mM, respectively. Photoirradiation to the solution was carried out using a 100 W tungsten lamp (Toshiba, ∼5000 Lx) equipped with an optical filter (λ > 430 nm, Toshiba Y-43 glass filter) at 25 °C. After irradiation, the enzymatic activity of CA for the *p*-nitrophenyl acetate hydrolysis was investigated at 25 °C in a 50 mM HEPES buffer (pH 7.2) containing 10% acetonitrile as mentioned above.

Emission and Lifetime Measurements. All the sample solutions were gently and carefully purged with N_2 gas for the emission lifetime measurements. Steady-state emission spectra were recorded on a Shimadzu RF-5300 instrument. Time-resolved emission spectra were measured by a single-photon counting method using a Horiba-Jobin Yvon TemPro. The instrumental response of the system to the excitation pulsed solid-state LED light source of 450 nm had a time width of about 100 ps and a repetition rate of about 100 MHz. The lifetime of the phosphorescence from the photoexcited $\{[Ru(bpy)(bpybs)]^{2+}\}^*$ was evaluated with software attached to this equipment.

Transient Absorption Measurements. To measure the transient absorption spectra, degassed solutions through several freeze–pump–thaw cycles in buffer solution were prepared. Nanosecond transient absorption measurements were carried out using a Unisoku TSP-1000-01 flash spectrometer system. A Q-switched Nd:YAG laser (Surelite I, Continuum) was employed for the flash photoirradiation, which generated the second harmonic 532 nm pulse of 6 ns duration (10 Hz). The tunable Optical Parametric Oscillators (OPO) system was used for producing the visible light (410–750 nm) when pumped with a Nd:YAG laser. A 150 W xenon arc lamp was used as the monitor light source. The time course of the absorbance decay was analyzed by single- or double-phase kinetics to determine the lifetime of the photoexcited state of $^3\{[Ru(bpy)(bpybs)]^{2+}\}^*$.

Other Measurements. Steady-state UV–vis spectra were measured with a Shimadzu UV-2550 instrument. ESI-mass spectra were measured with a JEOL JMS-T100LC AccuTOF instrument. All ^{1}H NMR spectra (400 MHz) were recorded on a JEOL JNM-AL400 FT-NMR instrument. ^{1}H NMR chemical shift values are reported in ppm as reference to the internal standard TMS. Cyclic voltammetry was done in N_2-saturated 0.050 M $[Bu_4N]ClO_4$ acetonitrile solutions by using an ALS Electrochemical Analyzer Model 610B instrument. A three-electrode system (BAS Inc.) was used with a Pt auxiliary electrode and a glassy carbon working electrode against a Ag/$AgClO_4$ (0.10 M $[Bu_4N]ClO_4$ in acetonitrile) reference electrode. The scan rate was 100 mV s^{-1}, and the potentials were calibrated by using 1,1′-dimethyl-4,4′-bipyridinediylium perchlorate, $[MV](ClO_4)_2$ {E^0 = −0.45 V vs NHE (normal hydrogen electrode)}. The pH's of the solutions were measured on a Hitachi-Horiba F-14RS pH meter.

■ ASSOCIATED CONTENT

Supporting Information

A PDF file containing steady-state absorption and emission spectra, emission lifetime data of the ruthenium(II) complexes, and UV–vis for enzymatic activity. This material is available free of charge via the Internet at http://pubs.acs.org.

AUTHOR INFORMATION

Corresponding Author

*Phone: +81-742-20-3391&3395. Fax: +81-742-20-3395. E-mail: hiroshi@cc.nara-wu.ac.jp (H.T.); tsukahara@cc.nara-wu.ac.jp (K.T.).

Notes

The authors declare no competing financial interest.

ACKNOWLEDGMENTS

This research was partly supported by Grant-in-Aid for Scientific Research No. 19550064 and 24550078 from the Ministry of Education, Culture, Sports, and Science and Technology (MEXT) of Japanese Government and Nara Women's University Intramural Grant for Project Research. The authors thank Professor Makoto Handa of Shimane University for elemental analyses.

REFERENCES

(1) McLendon, G.; Hake, R. Interprotein Electron Transfer. *Chem. Rev.* **1992**, *92*, 481−490.

(2) Bendall, D. S. *Protein Electron Transfer*; BIOS Scientific Publishers Ltd: Oxford, U.K., 1996.

(3) Nocek, J. M.; Zhou, J. S.; Forest, S. D.; Priyadarshy, S.; Beratan, D. N.; Onuchic, J. N.; Hoffman, B. M. Theory and Practice of Electron Transfer within Protein−Protein Complexes: Application to the Multidomain Binding of Cytochrome *c* by Cytochrome *c* Peroxidase. *Chem. Rev.* **1996**, *96*, 2459−2490.

(4) Gray, H. B.; Winkler, J. R. In *Electron Transfer in Chemistry*; Balzani, V., Ed.; Wiley-VCH: Weinheim, Germany, 2001; Vol. *3*, pp 3−23.

(5) Gray, H. B.; Winkler, J. R. Electron Tunneling through Proteins. *Q. Rev. Biophys.* **2003**, *36*, 341−372.

(6) Gray, H. B.; Winkler, J. R. In *Biological Inorganic Chemistry, Structure and Reactivity*; Bertini, I., Gray, H. B., Stiefel, E. I., Valentine, J. S., Eds.; University Science Books: Sausalito, CA, 2007; pp 261−277.

(7) Engels, F. In *Bioinorganic Photochemistry*; Stochel, G., Brindell, M., Macyk, W., Stasicka, Z., Szacilowski, K., Eds.; John Wiley & Sons: West Sussex, U.K., 2009; pp 209−226.

(8) (a) Hamachi, I.; Tanaka, S.; Shinkai, S. Light-Driven Activation of Reconstituted Myoglobin with a Ruthenium Tris(2,2′-bipyridine) Pendant. *J. Am. Chem. Soc.* **1993**, *115*, 10458−10459. (b) Hamachi, I.; Tanaka, S.; Tsukiji, S.; Shinkai, S.; Oishi, S. Design and Semisynthesis of Photoactive Myoglobin Bearing Ruthenium Tris(2,2′-bipyridine) Using Cofactor-Reconstitution. *Inorg. Chem.* **1998**, *37*, 4380−4388. (c) Hamachi, I.; Tsukiji, S.; Shinkai, S.; Oishi, S. Direct Observation of the Ferric-Porphyrin Cation Radical as an Intermediate in the Phototriggered Oxidation of Ferric- to Ferryl-Heme Tethered to $Ru(bpy)_3$ in Reconstituted Myoglobin. *J. Am. Chem. Soc.* **1999**, *121*, 5500−5506.

(9) Immoos, C. E.; Di Bilio, A. J.; Cohen, M. S.; Van der Veer, W.; Gray, H. B.; Farmer, P. J. Electron-Transfer Chemistry of Ru-Linker-(Heme)-Modified Myoglobin: Rapid Intraprotein Reduction of a Photogenerated Porphyrin Cation Radical. *Inorg. Chem.* **2004**, *43*, 3593−3596.

(10) McLendon, G.; Murphy, P. Metal Electronic Effects on Myoglobin Conformational Stability. *J. Biol. Chem.* **1980**, *255*, 4035−4039.

(11) (a) Zemel, H.; Hoffman, B. M. Long-range Triplet-Triplet Energy Transfer within Metal-Substituted Hemoglobins. *J. Am. Chem. Soc.* **1981**, *103*, 1192−1201. (b) Zhou, J. S.; Nocek, J. M.; DeVan, M. L.; Hoffman, B. M. Inhibitor-Enhanced Electron Transfer: Copper Cytochrome *c* as a Redox-Inert Probe of Ternary Complexes. *Science* **1995**, *269*, 204−207. (c) Liang, Z. X.; Nocek, J. M.; Kurnikov, I. V.; Beratan, D. N.; Hoffman, B. M. Electrostatic Control of Electron Transfer between Myoglobin and Cytochrome b_5: Effect of Methylating the Heme Propionates of Zn-Myoglobin. *J. Am. Chem. Soc.* **2000**, *122*, 3552−3553.

(12) Cowan, J. A.; Gray, H. B. Synthesis and Properties of Metal-Substituted Myoglobins. *Inorg. Chem.* **1989**, *28*, 2074−2078.

(13) (a) Pan, L. P.; Durham, B.; Wolinska, J.; Millett, F. Preparation and Characterization of Singly Labeled Ruthenium Polypyridine Cytochrome *c* Derivatives. *Biochemistry* **1988**, *27*, 7180−7184. (b) Durham, B.; Pan, L. P.; Long, J. E.; Millett, F. Photoinduced Electron-Transfer Kinetics of Singly Labeled Ruthenium Bis-(bipyridine) Dicarboxybipyridine Cytochrome *c* Derivatives. *Biochemistry* **1989**, *28*, 8659−8665. (c) Geren, L.; Hahm, S.; Durham, B.; Millet, F. Photoinduced Electron Transfer between Cytochrome *c* Peroxidase and Yeast Cytochrome *c* Labeled at Cys 102 with (4-Bromomethyl-4′-methylbipyridine)[bis(bipyridine)]ruthenium^{2+}. *Biochemistry* **1991**, *30*, 9450−9457. (d) Hahm, S.; Durham, B.; Millett, F. Photoinduced Electron Transfer between Cytochrome *c* Peroxidase and Horse Cytochrome *c* Labeled at Specific Lysines with (Dicarboxybipyridine)(bisbipyridine)ruthenium(II). *Biochemistry* **1992**, *31*, 3472−3477. (e) Millet, F.; Durham, B. Design of Photoactive Ruthenium Complexes To Study Interprotein Electron Transfer. *Biochemistry* **2002**, *41*, 11315−11324. (f) Engstrom, G.; Rajagukguk, R.; Saunders, A. J.; Patel, C. N.; Rajagukguk, S.; Merbitz-Zahradnik, T.; Xiao, K.; Pielak, G. J.; Trumpower, B.; Yu, C.-A.; Yu, L.; Curham, B.; Millett, F. Design of a Ruthenium-Labeled Cytochrome *c* Derivative to Study Electron Transfer with the Cytochrome bc_1 Complex. *Biochemistry* **2003**, *42*, 2816−2824.

(14) (a) Pletneva, E. V.; Fulton, D. B.; Kohzuma, T.; Kostíc, N. M. Protein Docking and Gated Electron-Transfer Reactions between Zinc Cytochrome *c* and the New Plastocyanin from the Fern *Dryopteris crassirhizoma*. Direct Kinetic Evidence for Multiple Binary Complexes. *J. Am. Chem. Soc.* **2000**, *122*, 1034−1046. (b) Tremain, S. M.; Kostíc, N. M. Fate of the Excited Triplet State of zinc Cytochrome *c* in the Presence of Iron(III), Iron(II), Iron-Free, and Heme-Free Forms of Cytochrome *c*. *Inorg. Chim. Acta* **2000**, *300*, 733−740.

(15) Hamachi, I.; Shinkai, S. Chemical Modification of the Structures and Functions of Proteins by the Cofactor Reconstitution Method. *Eur. J. Org. Chem.* **1999**, *1*, 539−549.

(16) (a) Hayashi, T.; Hisaeda, Y. New Functionalization of Myoglobin by Chemical Modification of Heme-Propionates. *Acc. Chem. Res.* **2002**, *35*, 35−43. (b) Hayashi, T. In *Handbook of Porphyrin Science with Applications to Chemistry, Physics, Material Science, Engineering, Biology and Medicine*; Kadish, K. M., Smith, K. M., Guilard, R., Eds.; World Scientific: Hackensack, NJ, 2010; Vol. *5*, pp 1−69.

(17) (a) Hu, Y.-Z.; Tsukiji, S.; Shinkai, S.; Oishi, S.; Hamachi, I. Construction of Artificial Photosynthetic Reaction Centers on a Protein Surface: Vectorial, Multistep, and Proton-Coupled Electron Transfer for Long-Lived Charge Separation. *J. Am. Chem. Soc.* **2000**, *122*, 241−253. (b) Hu, Y.-Z.; Takashima, H.; Tsukiji, S.; Shinkai, S.; Nagamune, T.; Oishi, S.; Hamachi, I. Direct Comparison of Electron Transfer Properties of Two Distinct Semisynthetic Triads with Non-Protein Based Triad: Unambiguous Experimental Evidences on Protein Matrix Effects. *Chem.—Eur. J.* **2000**, *6*, 1907−1916. (c) Hamachi, I.; Takashima, H.; Hu, Y.-Z.; Shinkai, S.; Oishi, S. Cyclodextrin-Appended Myoglobin as a Tool for Construction of a Donor−Sensitizer−Acceptor Triad on a Protein Surface. *Chem. Commun.* **2000**, 1127−1128. (d) Takashima, H.; Hu, Y.-Z.; Sano, K.; Shinkai, S.; Oishi, S.; Hamachi, I. Supramolecular Construction of Covalently and Nonconvalently-linked Photoinduced Electron Transfer System In Myoglobin Scaffold. *Electrochemistry* **2001**, *69*, 942−945.

(18) (a) Takashima, H.; Matsushima, Y.; Araki, Y.; Ito, O.; Tsukahara, K. Synthesis and Photophysical Properties of Zinc Myoglobin Appending an Ethidium Ion as a DNA Intercalator. *J. Biol. Inorg. Chem.* **2008**, *13*, 171−181. (b) Takashima, H.; Fujimoto, E.; Hirai, C.; Tsukahara, K. Synthesis and Spectroscopic Properties of Reconstituted ZincMyoglobin Appending a DNA-Binding Platinum-(II) Complex. *Chem. Biodiversity* **2008**, *5*, 2101−2112.

(19) Hayashi, T.; Takimura, T.; Ohara, Y.; Hitomi, Y.; Ogoshi, H. Photoinduced Electron Transfer from Zinc Porphyrin to a Linked

Quinone in Myoglobin. *J. Chem. Soc., Chem. Commun.* **1995**, 2503−2504.
(20) Heleg-Shabtai, V.; Gabriel, T.; Willner, I. Vectorial Photoinduced Electron-Transfer and Charge Separation in a Zn(II)-Protoporphyrin-Bipyridinium Dyad Reconstituted Myoglobin. *J. Am. Chem. Soc.* **1999**, *121*, 3220−3221.
(21) Takashima, H.; Tara, C.; Namikawa, S.; Kato, T.; Araki, Y.; Ito, O.; Tsukahara, K. Photoinduced Intramolecular Electron-Transfer Reactions of Reconstituted Met- and Zinc-Myoglobins Appending Acridine and Methylacridinium Ion as DNA-Binders. *J. Phys. Chem. B* **2006**, *110*, 26413−26423.
(22) Takashima, H.; Kawahara, H.; Kitano, M.; Shibata, S.; Murakami, H.; Tsukahara, K. Metal Ion-Dependent Fluorescent Dynamics of Photoexcited Zinc−Porphyrin and Zinc−Myoglobin Modified with Ethylenediaminetetraacetic Acid. *J. Phys. Chem. B* **2008**, *112*, 15493−15502.
(23) Thomas, C. M.; Ward, T. R. Artificial Metalloenzymes: Proteins as Hosts for Enantioselective Catalysis. *Chem. Soc. Rev.* **2005**, *34*, 337−346.
(24) Lo, K. K.; Lee, T. K. Luminescent Ruthenium(II) Polypyridine Biotin Complexes: Synthesis, Characterization, Photophysical and Electrochemical Properties, and Avidin-Binding Studies. *Inorg. Chem.* **2004**, *43*, 5275−5282.
(25) (a) Dunn, A. R.; Dmochowski, I. J.; Winkler, J. R.; Gray, H. B. Nanosecond Photoreduction of Cytochrome P450cam by Channel-Specific Ru-diimine Electron Tunneling Wires. *J. Am. Chem. Soc.* **2003**, *125*, 12450−12456. (b) Contakes, S. M.; Juda, G. A.; Langley, D. B.; Halpern-Manners, N. W.; Duff, A. P.; Dunn, A. R.; Gray, H. B.; Dooley, D. M.; Mitchell Guss, J.; Freeman, H. C. Reversible Inhibition of Copper Amine Oxidase Activity by Channel-Blocking Rutheniun-(II) and Rhenium(I) Molecular Wires. *Proc. Natl. Acad. Sci. U.S.A.* **2005**, *102*, 13451−13456. (c) Langley, D. B.; Brown, D. E.; Cheruzel, L. E.; Contakes, S. M.; Duff, A. P.; Hilmer, K. M.; Dooley, D. M.; Gray, H. B.; Mitchell Guss, J.; Freeman, H. C. Enantiomer-Specific Binding of Ruthenium(II) Molecular Wires by the Amine Oxidase of *Arthrobacter globiformis*. *J. Am. Chem. Soc.* **2008**, *130*, 8069−8078.
(26) Wilker, J. J.; Dmochowski, I. J.; Dawson, J. H.; Winkler, J. R.; Gray, H. B. Substrates for Rapid Delivery of Electrons and Holes to Buried Active Sites in Proteins. *Angew. Chem., Int. Ed.* **1999**, *38*, 89−92.
(27) Hess, C. R.; Juda, G. A.; Dooley, D. M.; Amil, R. N.; Hill, M. G.; Winkler, J. R.; Gray, H. B. Gold Electrodes Wired for Coupling with the Deeply Buried Active Site of *Arthrobacter globiformis* Amine Oxidase. *J. Am. Chem. Soc.* **2003**, *125*, 7156−7157.
(28) Ghosh, S.; Isaacs, L. Biological Catalysis Regulated by Cucurbit[7]uril Molecular Containers. *J. Am. Chem. Soc.* **2010**, *132*, 4445−4454.
(29) Hakansson, K.; Carlsson, M.; Svensson, L. A.; Liljas, A. Structure of Native and Apo Carbonic Anhydrase II and Structure of Some of Its Anion-Ligand Complexes. *J. Mol. Biol.* **1992**, *227*, 1192−1204.
(30) Saito, R.; Sato, T.; Ikai, A.; Tanaka, N. Structure of Bovine Carbonic Anhydrase II at 1.95 Å Resolution. *Acta Crystallogr., Sect. D: Biol. Crystallogr.* **2004**, *D60*, 792−795.
(31) Christianson, D. W.; Fierke, C. A. Carbonic Anhydrase: Evolution of the Zinc Binding Site by Nature and by Design. *Acc. Chem. Res.* **1996**, *29*, 331−339.
(32) (a) Supuran, C. T.; Scozzafava, A.; Casini, A. Carbonic Anhydrase Inhibitors. *Med. Res. Rev.* **2003**, *23*, 146−189. (b) Supuran, C. T.; Scozzafava, A.; Conway, J. *Carbonic Anhydrase − Its Inhibitors and Activators*; CRC Press: Boca Raton, FL, 2004. (c) Supuran, C. T. Carbonic Anhydrases: Novel Therapeutic Applications for Inhibitors and Activators. *Nat. Rev. Drug Discovery* **2008**, *7*, 168−181.
(33) (a) Elbaum, D.; Nair, S. K.; Patchan, M. W.; Thompson, R. B.; Christianson, D. W. Structure-Based Design of a Sulfonamide Probe for Fluorescence Anisotropy Detection of Zinc with a Carbonic Anhydrase-Based Biosensor. *J. Am. Chem. Soc.* **1996**, *118*, 8381−8387. (b) Fierke, C. A.; Thompson, R. B. Fluorescence-Based Biosensing of Zinc using Carbonic Anhydrase. *Biometals* **2001**, *14*, 205−222. (c) Thompson, R. B.; Cramer, M. L.; Bozym, R.; Fierke, C. A. Excitation Ratiometric Fluorescent Biosensor for Zinc Ion at Picomolar Levels. *J. Biomed. Opt.* **2002**, *7*, 555−560. (d) Bozym, R.; Thompson, R. B.; Stoddard, A. K.; Fierke, C. A. Measuring Picomolar Intracellular Exchangeable Zinc in PC-12 Cells Using a Ratiometric Fluorescence Biosensor. *ACS Chem. Biol.* **2006**, *1*, 103−111. (e) Bozym, R.; Hurst, T. K.; Westerberg, N.; Stoddard, A. K.; Fierke, C. A.; Frederickson, C. J.; Thompson, R. B. Determination of Zinc Using Carbonic Anhydrase-Based Fluorescence Biosensors. *Methods Enzymol.* **2008**, *450*, 287−309.
(34) Ciani, L.; Cecchi, A.; Temperini, C.; Supuran, C. T.; Ristori, S. Dissecting the Inhibition Mechanism of Cytosolic versus Transmembrane Carbonic Anhydrases by ESR. *J. Phys. Chem. B* **2009**, *113*, 13998−14005.
(35) Louie, A. Y.; Meade, T. J. Metal Complexes as Enzyme Inhibitors. *Chem. Rev.* **1999**, *99*, 2711−2734.
(36) (a) Roy, B. C.; Hegge, R.; Rosendahl, T.; Jia, X.; Lareau, R.; Mallik, S.; Srivastava, D. K. Conjugation of Poor Inhibitors with Surface Binding Groups: a Strategy to Improve Inhibition. *J. Chem. Soc., Chem. Commun.* **2003**, *18*, 2328−2329. (b) Banerjee, A. L.; Swanson, M.; Roy, B. C.; Jia, X.; Haldar, M.; Mallik, S.; Srivastava, D. K. Protein Surface-Assisted Enhancement in the Binding Affinity of an Inhibitor for Recombinant Human Carbonic Anhydrase-II. *J. Am. Chem. Soc.* **2004**, *126*, 10875−10883. (c) Roy, B. C.; Banerjee, A. L.; Swanson, M.; Jia, X.; Haldar, M.; Mallik, S.; Srivastava, D. K. Two-Prong Inhibitors for Human Carbonic Anhydrase II. *J. Am. Chem. Soc.* **2004**, *126*, 13206−13207. (d) Banerjee, A. L.; Eiler, D.; Roy, B. C.; Jia, X.; Haldar, M.; Mallik, S.; Srivastava, D. K. Spacer-Based Selectivity in the Binding of "Two-Prong" Ligands to Recombinant Human Carbonic Anhydrase I. *Biochemistry* **2005**, *44*, 3211−3224. (e) Jude, K. M.; Banerjee, A. L.; Haldar, M.; Manokaran, S.; Roy, B.; Mallik, S.; Srivastava, D. K.; Christianson, D. W. Ultrahigh Resolution Crystal Structures of Human Carbonic Anhydrases I and II Complexed with "Two-Prong" Inhibitors Reveal the Molecular Basis of High Affinity. *J. Am. Chem. Soc.* **2006**, *128*, 3011−3018.
(37) Rami, M.; Winum, J.-Y.; Innocenti, A.; Montero, J.-L.; Scozzafava, A.; Supuran, C. T. Carbonic Anhydrase Inhibitors: Copper(II) Complexes of Polyamino-polycarboxylamido aromatic/heterocyclic Sulfonamides are Very Potent Inhibitors of the Tumor-associated Isoforms IX and XII. *Bioorg. Med. Chem. Lett.* **2008**, *18*, 836−841.
(38) Vomasta, D.; Högner, C.; Branda, N. R.; König, B. Regulation of Human Carbonic Anhydrase I (hCAI) Activity by Using a Photochromic Inhibitor. *Angew. Chem., Int. Ed.* **2008**, *47*, 7644−7647.
(39) Gokhale, N. H.; Bradford, S.; Cowan, J. A. Catalytic Inactivation of Human Carbonic Anhydrase I by a Metallopeptide-Sulfonamide Conjugate is Mediated by Oxidation of Active Site Residues. *J. Am. Chem. Soc.* **2008**, *130*, 2388−2389.
(40) (a) Aaron, J. A.; Chambers, J. M.; Jude, K. M.; Costanzo, L. D.; Dmochowski, I. J.; Christianson, D. W. Structure of a ^{129}Xe-Cryptophane Biosensor Complexed with Human Carbonic Anhydrase II. *J. Am. Chem. Soc.* **2008**, *130*, 6942−6943. (b) Chambers, J. M.; Aru Hill, P.; Aaron, J. A.; Han, Z.; Christianson, D. W.; Kuzuma, N. N.; Dmochowski, I. J. Cryptophane Xenon-129 Nuclear Magnetic Resonance Biosensors Targeting Human Carbonic Anhydrase. *J. Am. Chem. Soc.* **2009**, *131*, 563−569.
(41) (a) Takaoka, Y.; Sakamoto, T.; Tsukiji, S.; Narazaki, M.; Matsuda, T.; Tochio, H.; Shirakawa, M.; Hamachi, I. Self-Assembling Nanoprobes that Display Off/On ^{19}F Nuclear Magnetic Resonance Signals for Protein Detection and Imaging. *Nat. Chem.* **2009**, *1*, 557−561. (b) Tsukiji, S.; Miyagawa, M.; Takaoka, Y.; Tamura, T.; Hamachi, I. Ligand-Directed Tosyl Chemistry for Protein Labeling *in vivo*. *Nat. Chem. Biol.* **2009**, *5*, 341−343. (c) Takaoka, Y.; Kiminami, K.; Mizusawa, K.; Matsuo, K.; Narazaki, M.; Matsuda, T.; Hamachi, I. Systematic Study of Protein Detection Mechanism of Self-Assembling ^{19}F NMR/MRI Nanoprobes toward Rational Design and Improved Sensitivity. *J. Am. Chem. Soc.* **2011**, *133*, 11725−11731. (d) Mizusawa, K.; Takaoka, Y.; Hamachi, I. Specific Cell Surface Protein Imaging by

Extended Self-Assembling Fluorescent Turn-on Nanoprobes. *J. Am. Chem. Soc.* **2012**, *134*, 13386−13395.
(42) (a) Balzani, V.; Juris, A.; Venturi, M.; Campagna, S.; Serroni, S. Luminescent and Redox-Active Polynuclear Transition Metal Complexes. *Chem. Rev.* **1996**, *96*, 759−834. (b) Campagna, S.; Puntoriero, F.; Nastasi, F.; Bergamini, G.; Balzani, V. Photochemistry and Photophysics of Coordination Compounds: Ruthenium. *Top. Curr. Chem.* **2007**, *280*, 117−214.
(43) (a) Tsukahara, K. Electron-Transfer Reactions of Metal Complexes and Iron Proteins with Viologen Radicals. *Trends Inorg. Chem.* **1991**, *2*, 17−32. (b) Takashima, H.; Tanaka, M.; Hasegawa, Y.; Tsukahara, K. Remarkably Stereoselective Photoinduced Electron-Transfer Reaction between Zinc Myoglobin and Optically Active Binaphthyl Bisviologen. *J. Biol. Inorg. Chem.* **2003**, *8*, 499−506.
(44) Thorslund, A.; Lindskog, S. Studies of the Esterase Activity and the Anion Inhibition of Bovine Zinc and Cobalt Carbonic Anhydrases. *Eur. J. Biochem.* **1967**, *3*, 117−123.
(45) Pocker, Y.; Stone, J. T. The Catalytic Versatility of Erythrocyte Carbonic Anhydrase. III. Kinetic Studies of the Enzyme-Catalyzed Hydrolysis of p-Nitrophenyl Acetate. *Biochemistry* **1967**, *6*, 668−678.
(46) Takaoka, Y.; Tsutsumi, H.; Kasagi, N.; Nakata, E.; Hamachi, I. One-Pot and Sequential Organic Chemistry on an Enzyme Surface to Tether a Fluorescent Probe at the Proximity of the Active Site with Restoring Enzyme Activity. *J. Am. Chem. Soc.* **2006**, *128*, 3273−3280.
(47) (a) Jain, A.; Huang, S. G.; Whitesides, G. M. Lack of Effect of the Length of Oligoglycine- and Oligo(ethylene glycol)-Derived para-Substituents on the Affinity of Benzenesulfonamides for Carbonic Anhydrase II in Solution. *J. Am. Chem. Soc.* **1994**, *116*, 5057−5062. (b) Chin, D.; Whitesides, G. M. Molecular Dynamics Simulations of $H_2NSO_2C_6H_4CONH(Gly)_3OBn$ Bound to the Active Site of Human Carbonic Anhydrase II. *J. Am. Chem. Soc.* **1995**, *117*, 6153−6164. (c) Krishnamurthy, V. M.; Bohall, B. R.; Semetey, V.; Whitesides, G. M. The Paradoxical Thermodynamic Basis for the Interaction of Ethylene Glycol, Glycine, and Sarcosine Chains with Bovine Carbonic Anhydrase II: An Unexpected Manifestation of Enthalpy/Entropy Compensation. *J. Am. Chem. Soc.* **2006**, *128*, 5802−5812. (d) Krishnamurthy, V. M.; Semetey, V.; Bracher, P. J.; Shen, N.; Whitesides, G. M. Dependence of Effective Molarity on Linker Length for an Intramolecular Protein-Ligand System. *J. Am. Chem. Soc.* **2007**, *129*, 1312−1320. (e) Krishnamurthy, V. M.; Kaufman, G. K.; Urbach, A. R.; Gitlin, I.; Gudiksen, K. L.; Weibel, D. B.; Whitesides, G. M. Carbonic Anhydrase as a Model for Biophysical and Physical-Organic Studies of Proteins and Protein-Ligand Binding. *Chem. Rev.* **2008**, *108*, 946−1051.
(48) (a) Tsukiji, S.; Wang, H.; Miyagawa, M.; Tamura, T.; Takaoka, Y.; Hamachi, I. Quenched Ligand-Directed Tosylate Reagents for One-Step Construction of Turn-On Fluorescent Biosensors. *J. Am. Chem. Soc.* **2009**, *131*, 9046−9054. (b) Mizusawa, K.; Ishida, Y.; Takaoka, Y.; Miyagawa, M.; Tsukiji, T.; Hamachi, I. Disassembly-Driven Turn-On Fluorescent Nanoprobes for Selective Protein Detection. *J. Am. Chem. Soc.* **2010**, *132*, 7291−7293.
(49) Di Bilio, A. J.; Crane, B. R.; Wehbi, W. A.; Kiser, C. N.; Abu-Omar, M. M.; Carlos, R. M.; Richards, J. H.; Winkler, J. R.; Gray, H. B. Properties of Photogenerated Tryptophan and Tyrosyl Radicals in Structurally Characterized Proteins Containing Rhenium(I) Tricarbonyl Diimines. *J. Am. Chem. Soc.* **2001**, *123*, 3181−3182.
(50) (a) Magnuson, A.; Frapart, Y.; Abrahamsson, M.; Horner, O.; Åkermark, B.; Sun, L.; Girerd, J.-J.; Hammarström, L.; Styring, S. A Biomimetic Model System for the Water Oxidizing Triad in Photosystem II. *J. Am. Chem. Soc.* **1999**, *121*, 89−96. (b) Sjödin, M.; Styring, S.; Åkermark, B.; Sun, L.; Hammarström, L. Proton-Coupled Electron Transfer from Tyrosine in a Tyrosine-Ruthenium-tris-Bipyridine Complex: Comparison with $Tyrosine_z$ Oxidation in Photosystem II. *J. Am. Chem. Soc.* **2000**, *122*, 3932−3936. (c) Pan, J.; Xu, Y.; Benkö, G.; Feyziyev, Y.; Styring, S.; Sun, L.; Åkermark, B.; Polivka, T.; Sundström, V. Stepwise Charge Separation from a Ruthenium-Tyrosine Complex to a Nanocrystalline TiO_2 Film. *J. Phys. Chem. B* **2004**, *108*, 12904−12910. (d) Sjödin, M.; Styring, S.; Wolpher, H.; Xu, Y.; Sun, L.; Hammarström, L. Switching the Redox Mechanism: Models for Proton-Coupled Electron Transfer from Tyrosine and Tryptophan. *J. Am. Chem. Soc.* **2005**, *127*, 3855−3863. (e) Irebo, T.; Reece, S. Y.; Sjödin, M.; Nocera, D. G.; Hammarström, L. Proton-Coupled Electron Transfer of Tyrosine Oxidation: Buffer Dependence and Parallel Mechanisms. *J. Am. Chem. Soc.* **2007**, *129*, 15462−15464. (f) Zhang, M.-T.; Hammarström, L. Proton-Coupled Electron Transfer from Tryptophan: A Concerted Mechanism with Water as Proton Acceptor. *J. Am. Chem. Soc.* **2011**, *133*, 8806−8809.
(51) Kalyanasundaram, K. Photophysics, Photochemistry and Solar Energy Conversion with Tris(bipyridyl)ruthenium(II) and Its Analogues. *Coord. Chem. Rev.* **1982**, *46*, 159−244.
(52) Reece, S. Y.; Seyedsayamdost, M. R.; Stubbe, J.; Nocera, G. G. Photoactive Peptides for Light-Initiated Tyrosyl Radical Generation and Transport into Ribonucleotide Reductase. *J. Am. Chem. Soc.* **2007**, *129*, 8500−8509.
(53) (a) McCafferty, D. G.; Bishop, B. M.; Wall, C. G.; Hughes, S. G.; Mecklenberg, S. L.; Meyer, T. J.; Erickson, B. W. Synthesis of Redox Derivatives of Lysine and Their Use in Solid-Phase Synthesis of a Light-Harvesting Peptide. *Tetrahedron* **1995**, *51*, 1093−1106. (b) Bishop, B. M.; McCafferty, D. G.; Erickson, B. W. 4′-Aminomethyl-2,2′-bipyridyl-4-carboxylic Acid (Abc) and Related Derivatives: Novel Bipyridine Amino Acids for the Solid-Phase Incorporation of a Metal Coordination Site Within a Peptide Backbone. *Tetrahedron* **2000**, *56*, 4629−4638.